# Identification of Pure Tones Radiated by Brushless D.C. Motors Used In Computer Disk Drives*

Ming-ran Lee; Rajendra Singh
*Department of Mechanical Engineering, The Ohio State University, 206 West 18th Avenue, Columbus, Ohio 43210-1107*

*Received: 18 June 1991; revised: 17 August 1992

The brushless D.C. motor is a primary source of noise in an idling computer disk drive. Typical acoustic measurements on a 3.5" hard disk drive reveal many pure tones with side bands over the frequency range from 1.3 to 6.1 kHz. New electromechanical noise source models have been developed to predict pure tones associated with the motor torque pulsations. Effects of motor winding, slots, inverter switching logic and mechanical defects have been studied. Numerical simulations are used to obtain analytic predictions and the results are compared with experimental data.

## Nomenclature

| | |
|---|---|
| $B$ | rotor flux density distribution (weber/m$^2$) |
| $\hat{B}$ | magnitude of rotor flux density (weber/m$^2$) |
| $B_m$ | angular viscous damping coefficient (N-m-s/rad) |
| $D$ | mean diameter of air gap (m) |
| $\mathbf{E}$ | back e.m.f. vector (v) |
| $\mathbf{I}$ | stator phase current vector (A) |
| $\hat{I}$ | magnitude of phase current (A) |
| $J$ | rotational inertia (kg-m$^2$/rad) |
| $K$ | Fourier coefficient |
| $\mathbf{L}$ | stator inductance matrix (H) |
| $L_{ij}$ | inductance between i-th and j-th state phases (H) |
| $L'$ | axial length of rotor (m) |
| $n$ | number of stator slots |
| $N_t$ | number of turns per phase winding |
| $P$ | number of poles on rotor |
| $\mathbf{R}$ | stator phase winding resistance matrix ($\Omega$) |
| $T$ | total motor torque (N-m) |
| $\bar{T}$ | mean value of motor torque (N-m) |
| $T_t$ | oscillating component of motor torque (N-m) |
| $\mathbf{V}$ | line-to-neutral stator phase voltage vector (v) |
| $W$ | total air gap energy (W) |
| $W_f$ | stored energy in magnetic field (W) |
| $x$ | slot width (m) |
| $y$ | slot gap (m) |
| $\delta$ | load angle (rad) |
| $\Delta$ | ratio of duration time in PWM scheme |
| $\Gamma$ | PWM pulse train |
| $\theta_r$ | angular position of rotor (rad) |
| $\omega_c$ | carrier frequency of PWM control scheme (rad/s) |
| $\Omega_r$ | angular velocity of rotor (rad/s) |
| $\bar{\Omega}_r$ | mean value of angular velocity of rotor (rad/s) |
| $\tau$ | switching period of PWM (s) |
| $\phi$ | phase angle of Fourier expansion (rad) |

Superscripts

| | |
|---|---|
| $E$ | harmonic associated with electric defect |
| $I$ | harmonic associated with imbalance |
| $M$ | harmonic associated with misalignment |

Subscripts

| | |
|---|---|
| $E$ | harmonic of back e.m.f. |
| $I$ | harmonic of phase current |
| V | harmonic of line-to-neutral phase voltage |
| $i,j$ | stator phase (a,b,c) |
| $q,s$ | harmonic indices of $P\Omega/2$ |
| $m$ | harmonic index of $\Omega_r$ |

## Introduction

The disk drive is a major source of noise in personal (desk-top or lap-top) computers and work stations as demonstrated by three experimental case histories.[1-3] Prasad *et. al.* measured the sound power of a disk drive in rotation and seeking modes. Several intense pure tones were noted, especially in the seeking operation.[1] According to them, radiated



Singh – 052

noise during the seeking mode was related to the design parameters of the stepper motor. Lutrell and Dunens examined various noise sources of two disk drive prototypes and reduced manufacturing related variations in sound levels.[2] In a recent experimental investigation, Woldemar and Kumano have found that tonal noise is amplified by motor or structural dynamics.[3] They successfully reduced the prominent high frequency tones by inserting foam material between the disk drive base and electronic circuit board, and by adding a varnish material to the motor coils. Based on these studies and other experimental data available to the authors, it is evident that the source mechanisms of such high frequency pure tones are poorly understood.[4] Also, disk drive acoustic behavior is yet to be characterized analytically. To remedy this situation, a comprehensive theoretical and experimental investigation has been undertaken by the authors. This paper presents preliminary results with an emphasis on the modeling of the electromechanical source of noise radiated by an idling disk drive. Main focus is on noise associated with motor torque pulsations; other noise source mechanisms are beyond the scope of this paper.

## Experimental Investigation

A 3.5" personal computer (PC) hard disk drive idling at a constant speed $\Omega$, (rad/s) is selected as an example case. A stack of disks is driven by an in-hub brushless d.c. motor (BDCM). The drive is driven by a typical PC power supply and is tested under two different conditions; with casing cover and without casing cover. First, the drive is evaluated without any other PC components being present. Second, the casing cover is removed from the disk drive and the in-hub motor is mounted on a rigid base built specifically for the experiment. The drive, as shown in Fig. 1, is suspended freely in a mini-anechoic chamber for sound pressure and structure acceleration measurements on a narrow band basis.

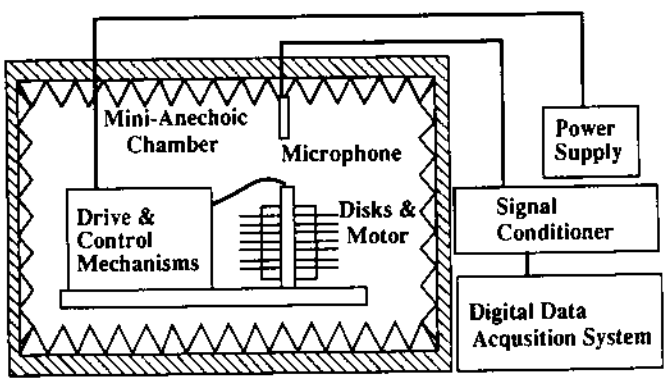


*Figure 1. Experimental set-up.*

In-situ intensity measurements, though not reported here, have been found to be similar to the free field data. Figure 2 shows a typical acceleration spectrum measured on the casing cover near the motor mounts. Numerous pure tones are clearly present over a wide range of frequencies. Figures 3 and 4 illustrate free field sound pressure spectra at 0.3 m above the disk with and without the casing cover, respectively. It is apparent that the noise below 1.3 kHz is inhibited or attenuated by the casing cover. However, several prominent pure tones with side band modulations are seen between 1.3 and 6.1 kHz even without the casing cover. Results for two disk drives (A and B) idling at 72 Hz are summarized in Table 1. Variations or uncertainties in the measured data under virtually the same conditions are observed. Frequency components and their amplitudes seem to be dependent on the electrical circuit control mechanisms, motor design parameters, thermal conditions, bearing characteristics, casing dynamics, assembly conditions and manufacturing variations.

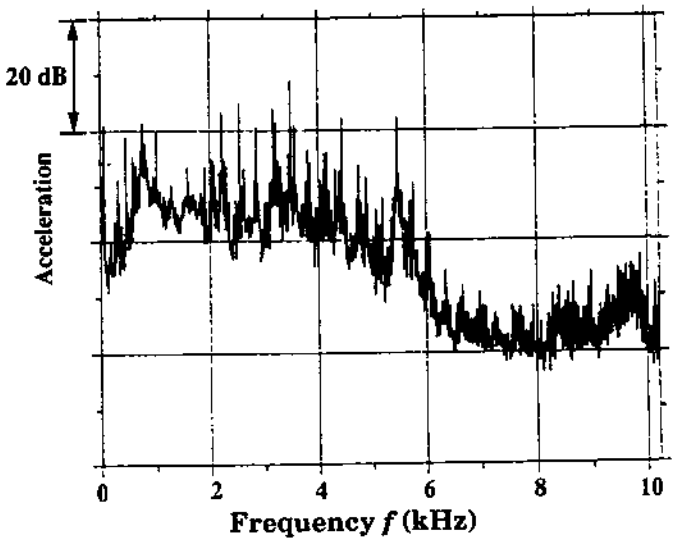


*Figure 2. Measured structural acceleration (in relative decibels) on the casing.*

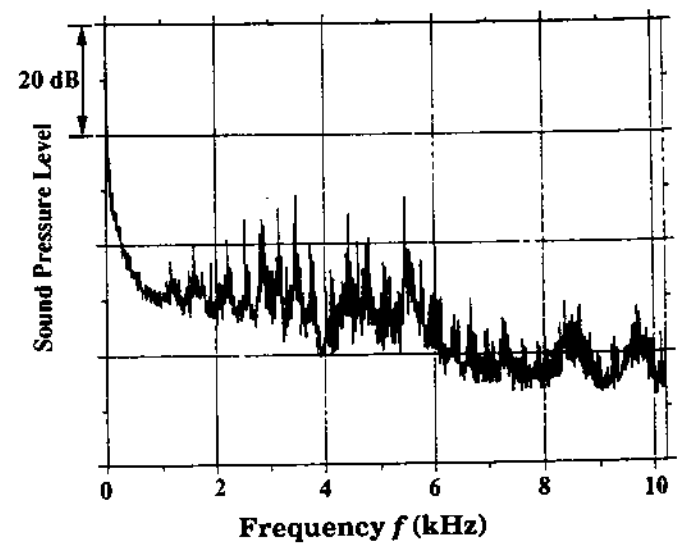


*Figure 3. Measured free field sound pressure level (in relative decibels) with casing cover.*

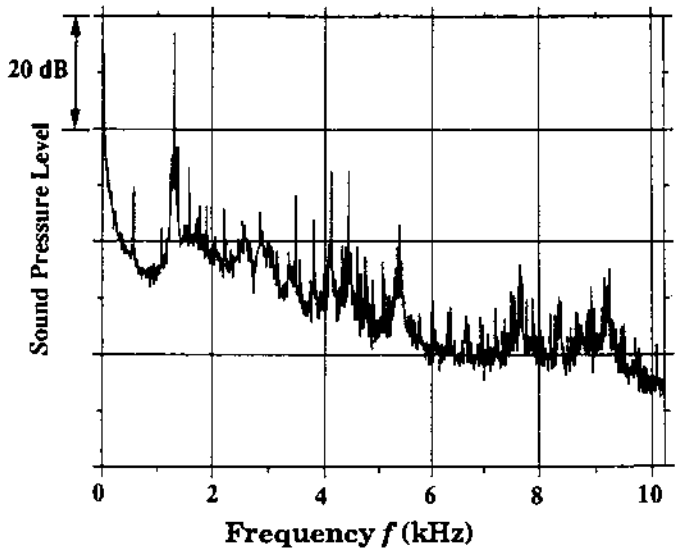


*Figure 4. Measured free field sound pressure level (in relative decibels) without casing cover.*

**Table 1. Measured dominant pure tones between 1.3 and 6.1 kHz and corresponding free field sound pressure levels (in relative decibels).**

| Drive A (with cover) | | | | Drive B (with cover) | | | | Drive B (without cover) | |
|---|---|---|---|---|---|---|---|---|---|
| Set A1* | | Set A2 | | Set B1* | | Set B2 | | Set B3 | |
| *f* (Hz) | dB | *f* (Hz) | dB | *f* (Hz) | dB | *f* (Hz) | dB | *f* (Hz) | dB |
| 1725 | 0 | 1736 | 0 | 1725 | 0 | 1584 | 0 | 1312 | 22 |
| 2225 | 0 | 2208 | 1 | 2550 | 10 | 2216 | 1 | 1584 | 0 |
| 2800 | 4 | 2840 | 0 | 3450 | 1 | 2536 | 5 | 2216 | -9 |
| 3450 | 1 | 3160 | 0 | 4600 | 2 | 2856 | 4 | 2856 | -9 |
| 5175 | 3 | 4312 | -1 | 5200 | 2 | 3168 | 6 | 3488 | -6 |
| 5475 | 5 | 5176 | 14 | 5475 | 5 | 3488 | 9 | 3808 | -9 |
| 5750 | 7 | 5464 | -5 | 5775 | 2 | 4440 | 6 | 4120 | -1 |
| 6050 | -1 | 5752 | -5 | 6050 | 0 | 5472 | 9 | 4440 | -1 |
| | | | | | | 6024 | -1 | 5392 | -10 |

* Data provided by the manufacturer.

## Analytical Formulation

The objective of this paper is to model the electromechanical noise source and to explain the emission of high frequency tones. Based on the experimental investigation and initial calculations, the following assumptions are made to simplify the analytical formulation of the idling disk: (1.) BDCM is the only source through rotor torque pulsation. (2.) Structure-borne paths are not included in the analysis. (3.) Disk dynamics, casing vibration and aerodynamic excitation are ignored. (4.) Thermal conditions do not affect the acoustic behavior of the source. (5.) Input d.c. voltage source is ideal and ripple free. (6.) Current inverters are ideal switches. (7.) Motor phase variables are balanced, each is offset by an electrical angle equal to $2\pi/3$. (8.) Rotor magnetomotive force (m.m.f.) wave is trapezoidal.[4] (9.) Torsional dynamics of the rotor can be given in terms of moment of inertia $J$ and damping coefficient $B_m$.

Three mathematical approaches have been employed previously to predict motor torque pulsation $T_r(t)$ either in time or frequency domain: phase variable formulation, Fourier series representation and d-q axis theory.[4-11] However, all of the available models are limited to the lower harmonics of $\Omega_r$ or to just a few higher harmonics. Accordingly, two new mathematical models are proposed to explain the disk drive acoustic behavior. In our approach the d-q axis theory is not used since it does not lead to high frequency response prediction in a convenient manner.

In this paper, two new mathematical models have been developed to predict harmonics of torque pulsations. The Phase Variable Formulation (Model I) retains the governing equations in the state space form. The inverter switching operation is simulated numerically and the induced voltage (back e.m.f.) is represented in terms of a piece-wise linear function of rotor angular position. This model employs essentially a numerical integration approach to solve the governing equations in time domain. An FFT algorithm is then used to predict the torque pulsation spectrum. The Fourier Series Representation (Model II) yields analytical expression for the steady state torque harmonics by expressing line-to-neutral phase voltage and back e.m.f. in terms of Fourier series. Fourier coefficients of phase current are obtained by using phase voltage equations. Consequently, the steady state torque harmonics are calculated directly by substituting Fourier coefficients of key variables into the electromagnetic torque equation. Model I provides more accurate predictions, however considerable computation time is needed for numerical solutions. Model II is obviously more efficient since it calculates the output torque directly in frequency domain.

## Model I [Phase Variable Formulation]

A typical 3-phase ($a$, $b$, and $c$ with Y connection) BDCM includes 6 pairs of current inverters as shown in Fig. 5. Each phase circuit consists of a winding resistance $R$, inductance $L_{ij}$ and back e.m.f., $E$. The input d.c. voltage is converted to nonsinusoidal a.c. voltage via an inverter switching logic and its amplitude is controlled using the pulse-width-modulation algorithm.[4,11] Phase voltage equations of the BDCM are given as follows where a bold letter implies a matrix/vector, $\mathbf{V}$ is the phase voltage, $\mathbf{I}$ is the phase current, $\underset{\sim}{\lambda}_r$ is the air gap flux linkage contributed by rotor, and $\underset{\sim}{\lambda}$ is the total air gap flux linkage.

$$\mathbf{V} = \mathbf{RI} + \underset{\sim}{\dot{\lambda}} \tag{1}$$

$$\underset{\sim}{\lambda} = \mathbf{LI} + \underset{\sim}{\lambda}_r \tag{2}$$

$$\mathbf{L} = \begin{bmatrix} L_{aa}(\theta_r) & L_{ab}(\theta_r) & L_{ac}(\theta_r) \\ L_{ab}(\theta_r) & L_{bb}(\theta_r) & L_{bc}(\theta_r) \\ L_{ac}(\theta_r) & L_{bc}(\theta_r) & L_{cc}(\theta_r) \end{bmatrix} \tag{3}$$

$$\mathbf{R} = \begin{bmatrix} R & 0 & 0 \\ 0 & R & 0 \\ 0 & 0 & R \end{bmatrix} \tag{4}$$

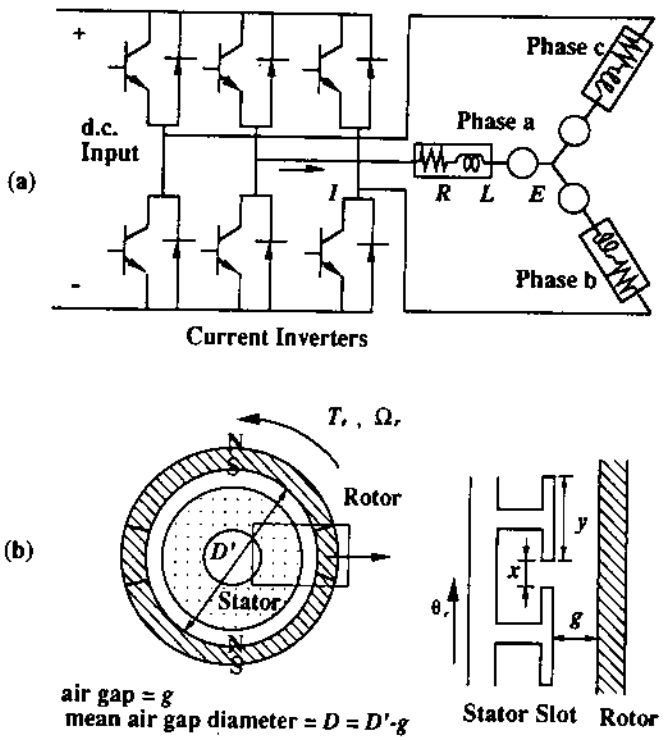


*Figure 5. Schematic of a 3-phase, 2-pole brushless d.c. motor (BDCM). (a) the current inverters and phase circuits and (b) the cross-sectional view of rotor and stator.*

Using Eqs. (1-4), one can obtain the governing equation of the electromagnetic circuits as given below by Eq. (5), where $\mathbf{E} = \dot{\lambda}_r$.

$$\dot{\mathbf{I}} = \mathbf{L}^{-1}[\dot{\mathbf{L}} + \mathbf{R}]\mathbf{I} + \mathbf{L}^{-1}[\mathbf{V} - \mathbf{E}] \tag{5}$$

Rotor dynamic equation is derived by relating the electromagnetic torque to rotational inertia and viscous damping effects as shown by Eq. (6) where $\theta_r = \int \Omega_r(t)dt$ is the angular position of rotor, $\bar{T}$ and $T_r$ are mean and fluctuating components of the motor output torque.

$$\begin{bmatrix} \dot{\theta}_r \\ \dot{\Omega}_r \end{bmatrix} = \begin{bmatrix} 0 & 1 \\ 0 & -B_m/J \end{bmatrix} \begin{bmatrix} \theta_r \\ \Omega_r \end{bmatrix} + \begin{bmatrix} 0 \\ (\bar{T}+T_r)/J \end{bmatrix} \tag{6}$$

Next, the output electromagnetic torque of a $P$-pole motor is derived by differentiating the stored energy in magnetic field with respect to rotor angular position.[11]

$$\bar{T} + T_r = \frac{d}{d\theta_r}[W_f(\mathbf{I},\theta_r)] \tag{7}$$

$$W_f(\mathbf{I},\theta_r) = \frac{P}{2}\left[\frac{1}{2}\mathbf{I}^T\mathbf{L}(\theta_r)\mathbf{I} + \mathbf{I}^T\lambda_r\right] \tag{8}$$

The equation of electromagnetic torque is thus expressed by

$$\bar{T} + T_r = \frac{P}{2}\left[\frac{1}{2}\mathbf{I}^T\left[\frac{d}{d\theta_r}\mathbf{L}(\theta_r)\right]\mathbf{I} + \frac{1}{\Omega_r}\mathbf{E}^T\mathbf{I}\right] \tag{9}$$

in which the back e.m.f. can be written by[5]

$$\mathbf{E}(\theta_r) = \frac{1}{2}N_r\Omega_r DL\mathbf{B}(\theta_r) \tag{10}$$

where $N_r$ is the number of turns per phase winding, $D$ is the mean air gap diameter, $L$ is the axial length of rotor, and $\mathbf{B}$ is the air gap flux density. The trapezoidal back e.m.f. $\mathbf{E}$ and quasi-square phase voltage $\mathbf{V}$ are expressed in terms of piece-wise linear curves and the expressions for $\mathbf{L}$ include the effects of dynamic imbalance, rotor misalignment, winding harmonics and saturation; these will be discussed later as a part of Model II. The spectral contents associated with the number of stator slots are formulated by differentiating the stored energy in the air gap field associated with the modulated rotor flux distribution with respect to the rotor angle.[5] Assume that trapezoidal rotor flux density is modulated by stator slots as shown in Fig. 6. Then, the stored energy between any slot can be expressed by[5]

$$\Delta W_k(\theta_r) = \frac{DgL}{2}\int_{\alpha_1}^{\alpha_2}\frac{1}{2\mu_0}\left(1+\frac{x}{y}\right)^2 B^2(\theta,)d\theta_r \; ; \tag{11a-c}$$

$$\alpha_1 = \theta_r + \frac{x}{D} + \frac{2k\pi}{n}\;,\quad \alpha_2 = \theta_r + \frac{x+2y}{D} + \frac{2k\pi}{n}$$

where, $x$ is the slot width and $y$ is the gap of slot opening. The total air gap energy $W$ is thus the summation of stored energy over $n$ slots.

$$W(\theta_r) = \sum_{k=1}^{n}\Delta W_k(\theta_r) \tag{12}$$

Consequently, the torque pulsation due to open stator slots ($T_r$) is

$$T_r = \frac{dW}{d\theta_r} \tag{13}$$

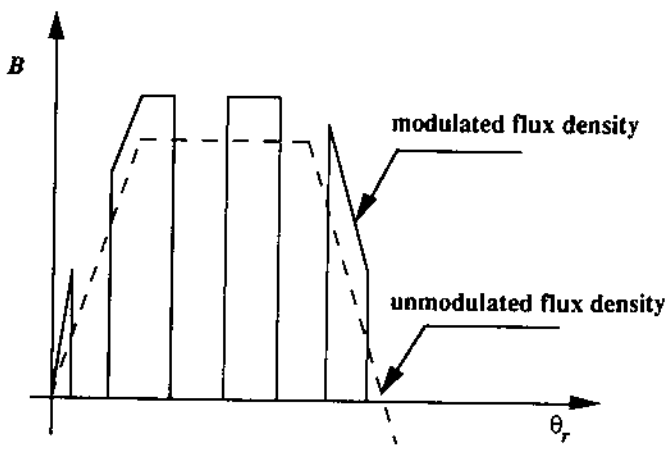


*Figure 6. Air-gap flux density distribution modulated by open stator slots.*

Since this analytical differentiation expression causes significant numerical errors, the effect of $T_r$ was not considered in the computer simulation of Model I. It will be proven later by using Model II that the fundamental frequency of $T_r$ is given by the product of slot number and rotor pole pair number. Therefore, such torque harmonics can be

predicted even without a computer simulation model. Model I is solved by using the direct time domain integration techniques.[6,7] An FFT algorithm is then used to determine the torque pulsation spectrum $T_e(f)$ where $f$ is the frequency in Hz.

The pulse-width-modulation (PWM) switching control algorithm is studied separately from this model in order to simplify the overall problem. It is seen that the switching operation induces another family of harmonics with the fundamental frequency equal to the carrier frequency. Figure 7 shows typical simulation results of an 8-pole, 3-phase BDCM with constant inductances operated under a fixed-rate PWM switching logic. The fixed PWM switching rate was selected to be 24 times the electrical frequency ($P\Omega_r/2$); therefore, the dominant tone is at 96 $\Omega_r$ which is the same as the carrier frequency.

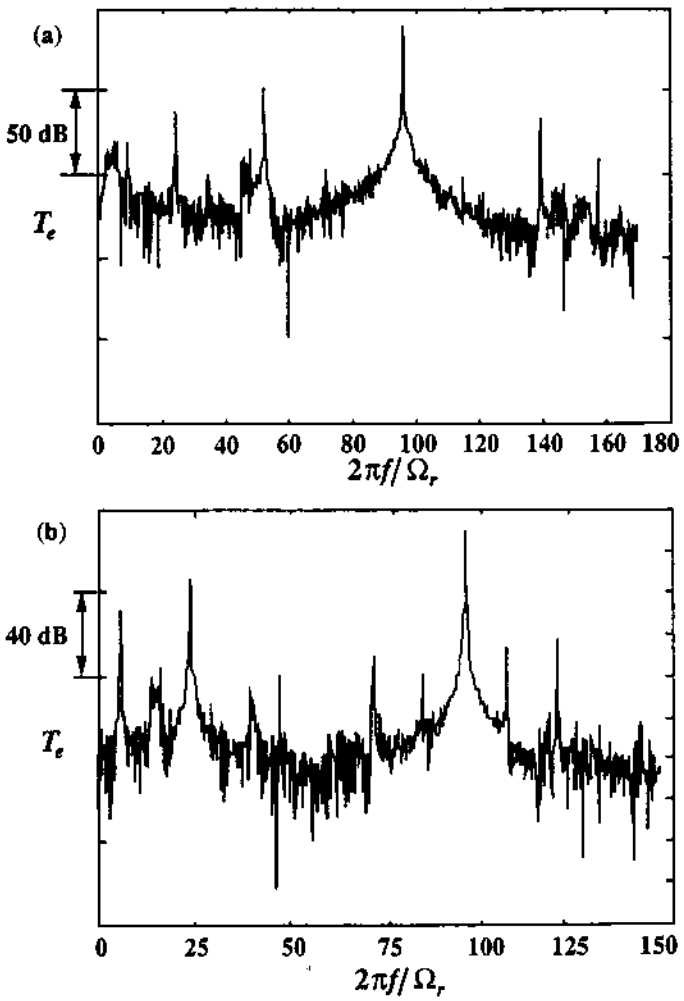


*Figure 7. Motor torque pulsations generated by the PWM switching: (a) 120° discrete type switching logic. (b) 180° continuous type switching logic.*

## Model II [Fourier Series Representation]

For a three-phase machine, the phase voltage $V_a$ and back e.m.f. $E_a$ of the first phase ($a$) can be expressed by

$$E_a = \sum_{q=odd}^{\infty} K_{E,qP/2} \exp\left(jq\frac{P}{2}\theta_r\right) \tag{14}$$

$$V_a = \sum_{q=odd}^{\infty} K_{V,qP/2} \exp\left[jq\frac{P}{2}(\theta_r-\delta)\right] \tag{15}$$

where $\delta$ represents the load angle which is the phase lead angle of the stator m.m.f. wave relative to the rotor m.m.f. wave. For assumed trapezoidal back e.m.f. E and quasi-square line-to-neutral phase voltage V functions of the rotor angular position $\theta_r$ as shown in Fig. 8, the Fourier coefficients can be expressed as follows

$$K_{E,qP/2} = \frac{4N_r\Omega_r DL\cdot\hat{B}}{\pi q^2\beta}\sin\left(\frac{q\beta}{2}\right) \tag{16}$$

$$K_{V,qP/2} = \frac{2V_{dc}}{q\pi}\cos\left(\frac{q\pi}{6}\right) \tag{17}$$

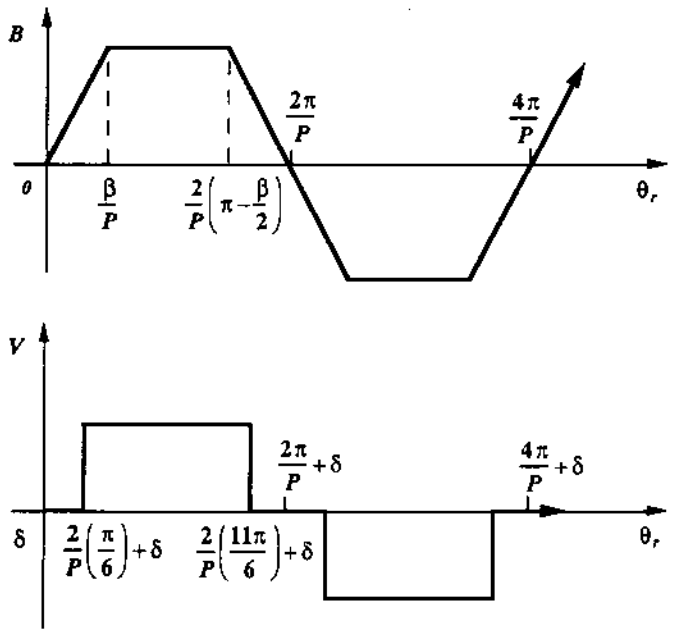


*Figure 8. Assumed trapezoidal rotor flux density distribution and the quasi-square line-to-neutral phase voltage.*

Since phase variables are assumed to be balanced, corresponding formulations for phases $b$ and $c$ are obtained by substituting $\theta_r$ with $\theta_r-(4\pi/3P)$ and $\theta_r+(4\pi/3P)$, respectively, where $P$ is the number of rotor poles. Fourier coefficients for each phase current can now be calculated by employing Eqs. (1-5). In order to simplify this formulation, only mean values of self ($\bar{L}$) and mutual ($\bar{M}$) inductances are included, only those harmonics of current which are related to the harmonics of input voltage and back e.m.f. are considered in the cal-

culation of $T_r(t)$. In addition to the mean inductance term $L$, rotor imbalance and drive misalignment effects are introduced through $L^I$ and $L^M$, respectively, as shown below where $K_L$ represents the Fourier coefficient of self inductance. Similarly, electrical defects of the inductance are modeled via the $L^E$ term as given below. Therefore the total self inductance of phase $a$ is

$$L_{aa}(\theta_r) = \bar{L} + L^I(\theta_r) + L^M(\theta_r) + L^E(\theta_r) \tag{18}$$

$$L^I(\theta_r) = \sum_{m=1}^{\infty} K^I_{L,m}\exp(jm\theta_r) \tag{19}$$

$$L^M(\theta_r) = \sum_{m=1}^{\infty} K^M_{L,2m}\exp(j2m\theta_r) \tag{20}$$

$$L^E(\theta_r) = \sum_{m=1}^{\infty} K^E_{L,Pm}\exp(jPm\theta_r) \tag{21}$$

Self inductances for phases $b$ and $c$ are expressed using the substitution of $\theta_r$ as defined earlier for $E_a$ and $V_a$. Similarly, the mutual inductance $L_{ac}$ between phases $b$ and $c$, flux link of state phase $b$ due to current of state phase $c$, is derived as follows where $K_M$ is the Fourier coefficient associated with mutual inductance.

$$L_{ac}(\theta_r) = \bar{M} + \sum_{m=1}^{\infty}\left[K^I_{M,m}\exp(jm\theta_r) + K^M_{M,2m}\exp(j2m\theta_r) + K^E_{M,Pm}\exp(jPm\theta_r)\right] \tag{22}$$

Next, $L_{ab}(\theta_r)$ and $L_{ab}(\theta_r)$ are obtained by substituting $\theta_r$ with $\theta_r-(4\pi/3P)$ and $\theta_r+(4\pi/3P)$, respectively. Substituting Eqs. (14-22) into Eq. (9), the torque pulsation $T_r(t)$ can be written explicitly in the Fourier series form. After a considerable analytical manipulation, the final expression of output torque pulsations is found to be as follows:

$$\begin{aligned}
T_r(t) = {} & \frac{3}{2\Omega_r}\sum_{\substack{s,q\\ odd}}^{\infty}\left[K_{I,sP2}K_{B,qP2}\left\{A_1\cos\left[\frac{P}{2}(s+q)\theta_r+\phi_{sP2}+\phi_{qP2}\right]+A_2\cos\left[\frac{P}{2}(s-q)\theta_r-\phi_{sP2}+\phi_{qP2}\right]\right\}\right. \\
& -\frac{3}{4}\sum_{m,q,s}^{\infty} mK_{L,m}K_{I,sP2}K_{I,qP2}\left\{B_1\sin\left[\frac{P}{2}\left(\frac{2}{P}m+s+q\right)\theta_r+\left(\phi_{sP2}+\phi_{qP2}\right)\right]\right. \\
& \quad +B_2\sin\left[\frac{P}{2}\left(\frac{2}{P}m-s-q\right)\theta_r-\left(\phi_{sP2}+\phi_{qP2}\right)\right] \\
& \quad +B_3\sin\left[\frac{P}{2}\left(\frac{2}{P}m+s-q\right)\theta_r+\left(\phi_{sP2}-\phi_{qP2}\right)\right] \\
& \quad \left.+B_4\sin\left[\frac{P}{2}\left(\frac{2}{P}m-s+q\right)\theta_r-\left(\phi_{sP2}-\phi_{qP2}\right)\right]\right\} \\
& -\frac{1}{4}\sum_{m,q,s}^{\infty} mK_{M,m}K_{I,sP2}K_{I,qP2}\left\{\sin\left[\frac{P}{2}\left(\frac{2}{P}m+s+q\right)\theta_r+\left(m-\frac{P}{2}q\right)\frac{2\pi}{3}+\left(\phi_{sP2}+\phi_{qP2}\right)\right]\right. \\
& \quad +\sin\left[\frac{P}{2}\left(\frac{2}{P}m-s-q\right)\theta_r+\left(m+\frac{P}{2}q\right)\frac{2\pi}{3}+\left(\phi_{sP2}-\phi_{qP2}\right)\right] \\
& \quad +\sin\left[\frac{P}{2}\left(\frac{2}{P}m+s-q\right)\theta_r+\left(m+\frac{P}{2}q\right)\frac{2\pi}{3}-\left(\phi_{sP2}-\phi_{qP2}\right)\right] \\
& \quad \left.+\sin\left[\frac{P}{2}\left(\frac{2}{P}m-s+q\right)\theta_r+\left(m-\frac{P}{2}q\right)\frac{2\pi}{3}-\left(\phi_{sP2}-\phi_{qP2}\right)\right]\right\} \\
& -\frac{1}{4}\sum_{m,q,s}^{\infty} mK_{M,m}K_{I,sP2}K_{I,qP2}\left\{\sin\left[\frac{P}{2}\left(\frac{2}{P}m+s+q\right)\theta_r-\left(s-q\right)\frac{P\pi}{3}+\left(\phi_{sP2}+\phi_{qP2}\right)\right]\right. \\
& \quad +\sin\left[\frac{P}{2}\left(\frac{2}{P}m-s-q\right)\theta_r+\left(s-q\right)\frac{P\pi}{3}-\left(\phi_{sP2}+\phi_{qP2}\right)\right] \\
& \quad +\sin\left[\frac{P}{2}\left(\frac{2}{P}m+s-q\right)\theta_r-\left(s+q\right)\frac{P\pi}{3}+\left(\phi_{sP2}-\phi_{qP2}\right)\right] \\
& \quad \left.\left.+\sin\left[\frac{P}{2}\left(\frac{2}{P}m-s+q\right)\theta_r+\left(s+q\right)\frac{P\pi}{3}-\left(\phi_{sP2}-\phi_{qP2}\right)\right]\right\}
\end{aligned} \tag{23}$$

where, $s$ and $q$ are odd number, $\phi_i$ is the phase angle of Fourier expansions of current, and

$$A_1 = \begin{cases}1 & s+q = 3k\\ 0 & \text{otherwise}\end{cases} \qquad A_2 = \begin{cases}1 & |s-q| = 3k\\ 0 & \text{otherwise}\end{cases}$$

$$B_1 = \begin{cases}1 & m+s+q = 3k\\ 0 & \text{otherwise}\end{cases} \qquad B_2 = \begin{cases}1 & |m-s-q| = 3k\\ 0 & \text{otherwise}\end{cases}$$

$$B_3 = \begin{cases}1 & |m+s-q| = 3k\\ 0 & \text{otherwise}\end{cases} \qquad B_4 = \begin{cases}1 & |m-s+q| = 3k\\ 0 & \text{otherwise}\end{cases}$$

Torque $T_r(t)$ associated with the fluctuating flux is derived by substituting Fourier series of machine variables into Eqs. (11-13). The final expression is given below where $K_{B,qP2}$ is the Fourier coefficient of rotor flux density distribution and $g$ is the air gap.

$$T_r(t) = \frac{nDLg}{4\mu_0}\left(1+\frac{x}{y}\right)^2\sum_{q,odd}^{\infty}(K_{B,qP2})^2\left\{\sin\left[qn\left(\frac{P}{2}\theta_r+\frac{x+2y}{D}\right)\right]-\sin\left[qn\left(\frac{P}{2}\theta_r+\frac{x}{D}\right)\right]\right\} \tag{24}$$

To simulate the PWM control algorithm operation, the phase voltage in Model II is multiplied with a pulse train $\Gamma(t)$ of unit magnitude.[12] In order to simplify this phenomenon, the period $\tau = 2\pi/\omega_c$ of pulse train is assumed to be fixed as shown in Fig. 9. Consequently, the Fourier series of the pulse train is expressed as follows:

$$\Gamma(t) = \Delta + \sum_{n=1}^{\infty}\frac{1}{n\pi}\left\{\sin(2n\pi\Delta)\cos(n\omega_c t) + [1-\cos(2n\pi\Delta)]\sin(n\omega_c t)\right\} \tag{25}$$

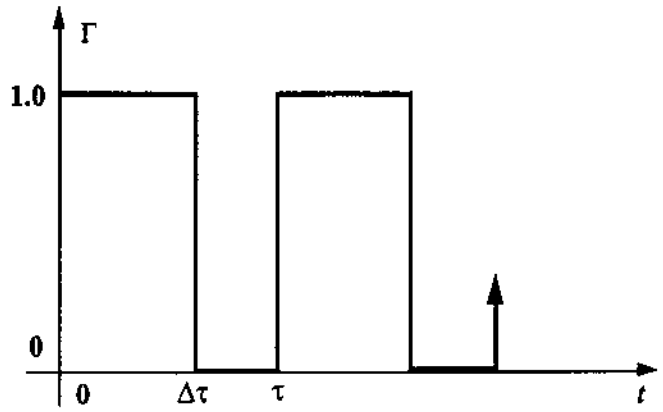


*Figure 9. PWM pulse train of period τ.*

Finally, the spectral contents of torque consist of four groups, as expressed below functionally and identified clearly in Table 2.

$$T_e(t) = \sum_{q=1}^{\infty}\sum_{\alpha=0}^{\infty} F_1[(3qP\Omega_r \pm \alpha\omega_c)t] + \sum_{s=\text{odd}}^{\infty} F_2(0.5snP\Omega_r t)$$

$$+\sum_{q=1}^{\infty}\sum_{m=k,2k,\ldots}^{\infty}\sum_{\alpha=0}^{\infty} F_3[(qP\Omega_r \pm m\Omega_r \pm \alpha\omega_c)t] \qquad (26)$$

The rotor angular velocity $\Omega_r$ has been assumed to be constant in our analyses. In practice, $\Omega_r$ also contains ripples due to the pulsating torque. To include this effect, $\Omega_r$ needs to be decomposed into a mean angular velocity and an oscillating speed with the amplitude equal to the zero-to-peak value of given velocity ripple. Then, the Jocobi expansion has to be applied to the above torque formulation. Since the pulsating amplitude in the steady state is much smaller compared to the mean angular velocity as shown in Fig. 10, it can be ignored.

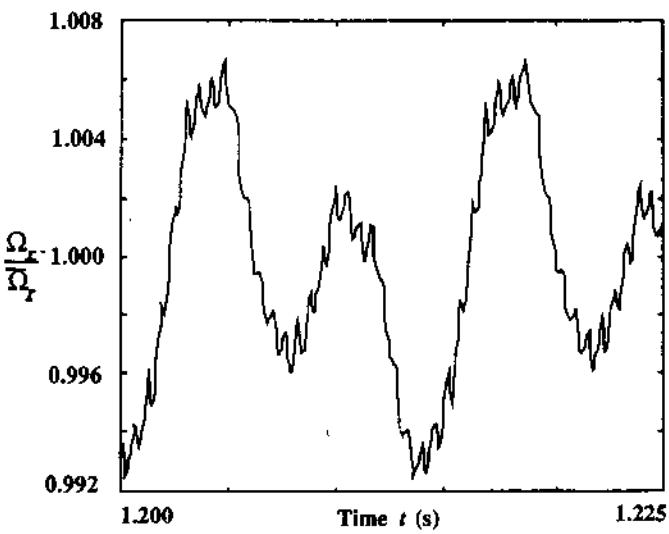


*Figure 10. Normalized rotor angular velocity fluctuation.*

**Table 2. Harmonics of motor torque (as yielded by Model II)**

| | Harmonic Group | Frequency Contents | Source |
|---|---|---|---|
| Without Pulse-Width-Modulation (PWM) | (i) | harmonics of $3P\Omega_r$ | dynamic interactions between E and I |
| | (ii) | odd harmonics of $0.5nP\Omega_r$ | open stator slot |
| | (iii) | $sP\Omega_r + m\Omega_r$ where $s$ is an integer and $m=q, 2q, Pq; q=1, 2, 3, \cdots$. | inductance variation |
| With Pulse-Width-Modulation (PWM) | (i) | $3qP\Omega_r \pm \alpha\omega_c$ where $q=1,2,3,\cdots$ and $\alpha=0,1,2,\cdots$. | dynamic interactions between E and I with side bands generated by PWM |
| | (ii) | odd harmonics of $0.5nP\Omega_r$ | open stator slot |
| | (iii) | $sP\Omega_r \pm m\Omega_r \pm \alpha\omega_c$ where $s$ is an integer, $\alpha=0,1,2,\cdots$ and $m=q, 2q, Pq; q=1, 2, 3, \cdots$. | inductance variation with side bands generated by PWM |
| | (vi) | harmonics of $\omega_c$ | carrier frequency $\omega_c$ |

## Results and Conclusion

Numerical data set used to illustrate the application of both models is given in Table 3. Note that several motor parameters are estimated by trial and error to match the given operating conditions of the sample disk drive. Since the PWM control scheme is not known sufficiently, it is not included in subsequent calculations. Only the first three harmonics of $L_l$, $L_M$ and $L_s$ terms in Eqs. (18-22) are included in the predictions yielded by Model II.

**Table 3. Data set used for analysis.**

| Parameter | Symbol | Value |
|---|---|---|
| number of rotor magnetic poles | $P$ | 8 |
| mean rotor rotation speed | $\Omega_r/2\pi$ | 72 Hz |
| number of stator slots | $n$ | 9 |
| number of turns per phase windings | $N$ | 141 |
| phase resistance | $R$ | 2.2 Ω |
| mean self inductance | $\bar{L}$ | 0.000147 H |
| mean mutual inductance | $\bar{M}$ | 0.00005 H |
| axial length of rotor | $L_r$ | 0.013 m |
| mean diameter of air gap | $D$ | 0.0181 m |
| air gap | $g$ | 0.00019 m |
| width of slot opening | $x$ | 0.00104 m |
| width of slot face | $y$ | 0.00513 m |
| amplitude of d.c. voltage source | $V_{dc}$ | 12 V |

Steady state time histories of phase current and torque, as yielded by Model I, are shown in Fig. 11. Torque pulsation spectra T(*f*) as predicted by Models I and II for the sample case are shown in Fig. 12. The most dominant peak corresponds to $3P\ \Omega_r$ and it has been taken as the reference (0 dB) for both spectra. Only those peaks whose amplitudes are greater than -50 dB are retained for analysis. Even though the frequency range of interest is restricted, spectral predications are given from 0 to 10 kHz. Both models match with each other reasonably well. Discrepancies are due to the fact

that Model II represents an analytical approximation to the solution; also, numerical solution and FFT algorithm errors are present in Model I.

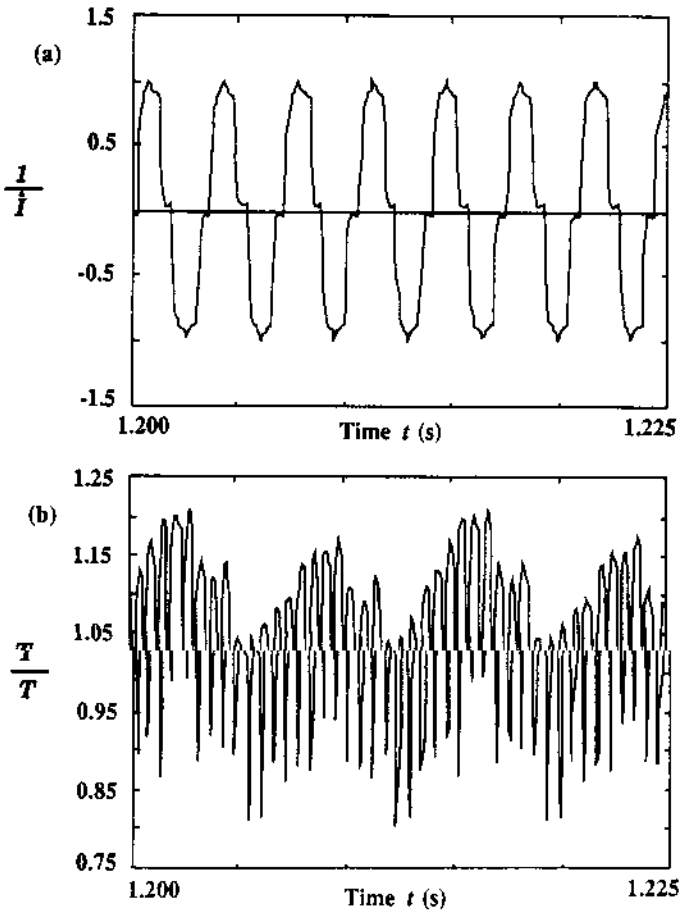


*Figure 11. Steady state time histories predicted by Model I. (a) normalized phase current. (b) normalized motor torque.*

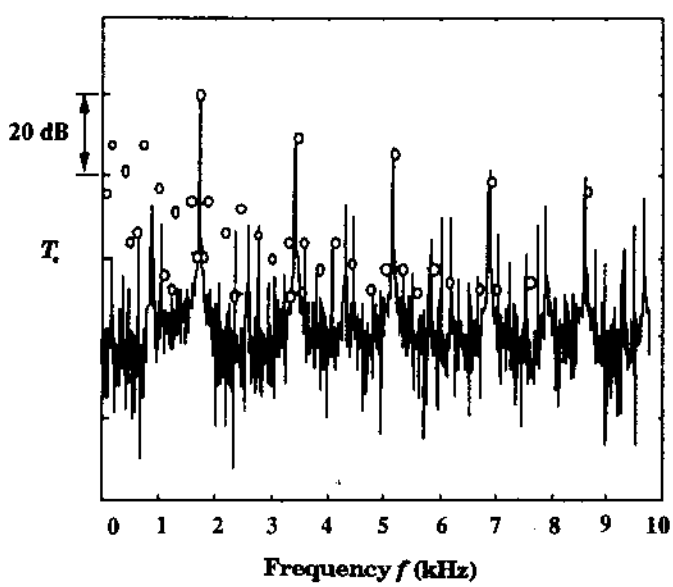


*Figure 12. Motor torque pulsation T(f) predictions (in relative decibels) by using Model I ( — ) and Model II ( o ).*

Measured and predicted pure tones are compared in Fig. 13. Even though a number of simplifications have been made in our noise source model, most (if not all) of the pure tones are predicted consistently either by Model I or II. Various harmonics of $\Omega_r$ as discussed earlier are also identified in Fig. 13. Chief among these are $3P$, $6P$ and $9P$ from group (i), $0.5nP$ from group (ii), and $2P+2$, $3P-2$, $4P-2$, $7P+1$, $8P-4$, $8P-2$ and $10P+4$ from group (iii). Given these results and especially an encouraging correlation between theory and experiment, one can conclude that the frequencies associated with motor torque pulsation coincide with the frequencies of pure tones. Nonetheless, the models presented here are incapable of explaining all of the available experimental data and other empirical observations since noise transmission paths and radiating surface(s) are yet to be included in our theory.[1] Further analytical work will consider these and our models are expected to resolve a few perplexing aspects of the disk drive acoustic behavior. Our formulations can also be extended to examine the noise source characteristics of other 3-phase electrical machines and motion control devices used in a variety of consumer and industrial products.

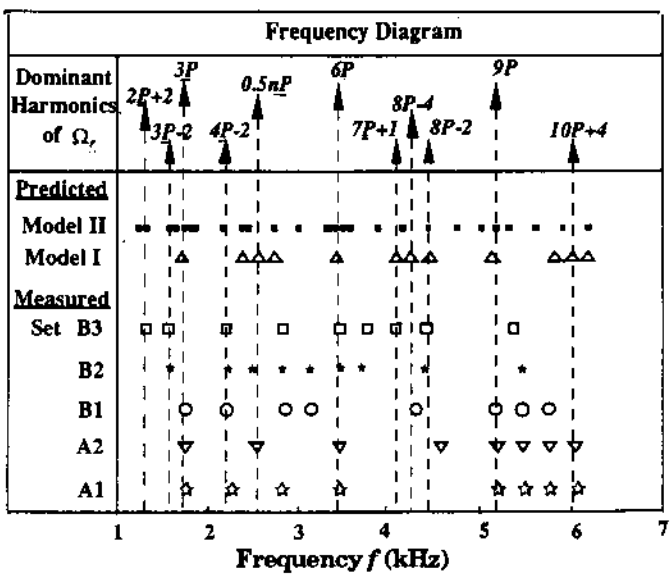


*Figure 13. Comparison of measured and predicted pure tones given $\Omega_r/2\pi$ = 72 Hz, P = 8 and n = 9. Also refer to Table 1 and Figs. 2-4 and 12.*

## Acknowledgement

The authors would like to thank the IBM Corporation for supporting this study.

## References

1. M. G. Prasad, D. Quinlan and G. Elko, "Noise and Vibration Studies of Small Winchester Disk Drives," *Proceedings of the 1987 National Conference on Noise Control Engineering*, Jiri Tichy, Ed. (Institute of Noise Control Engineering, Poughkeepsie, NY, 1987) pp. 147-152.

2. L. F. Luttrell and E. K. Dunens, "Noise Sources in Disk Drives," *Proceedings of the 1987 National Conference on Noise Control Engineering*, Jiri Tichy, Ed. (Institute of Noise Control Engineering, Poughkeepsie, NY, 1987) pp. 141-146.

3. C. M. Woldemar and A. Kumano, "Noise Control of Disc Drives for Desk-Top Computers," *Proceedings of the 1990 National Conference on Noise Control Engineering*, Ilene J. Busch-Vishniac, Ed. (Institute of Noise Control Engineering, Poughkeepsie, NY, 1990) pp. 89-94.

4. Personal conversations with computer disk drive engineers (1990).

5. H. R. Bolton, Y. D. Liu and N. M. Mallinson, "Investigation into a Class of Brushless DC Motor with Quasisquare Voltages and Currents," *IEE Proc. Pt. B, Electric Power Applications*, **133**(2), pp. 103-111, March (1986).

6. P. Pillay and R. Krishnan, "Modeling, Simulation, and Analysis of Permanent-Magnet Motor Drives, Part II: The Brushless DC Motor Drive," *IEEE Tran. on Industry Applications*, **25**(2), pp. 274-279, March/April (1989).

7. Y. Murai, et. al., "Torque Ripple Improvement for Brushless DC Miniature Motors," *IEEE Tran. on Industry Applications*, **25**(3), pp. 441-450, May/June (1989).

8. H. R. Bolton and R. A. Ashen, "Influence of Motor Design and Feed-Current Waveform on Torque Ripple in Brushless DC Drives," *IEE Proc., Pt. B*, **131**(3), pp. 82-90, May (1984).

9. P. M. Hart and W. J. Bonwick, "Harmonic Modelling of Synchronous Machines," *IEE Proc. Pt. B*, **135**(2), pp. 52-58, March (1988).

10. E. Goodman, "Torque, Voltage, and Current Harmonics of Synchronous Machines," *IEEE Tran. on Industry Application*, **20**(1), pp. 209-215, Jan./Feb. (1984).

11. P. C. Krause and O. Wasynczuk, *Electromechanical Motion Devices*, McGraw-Hill, New York (1989).

12. G. A. Kaufman and A. B. Plunkett, "Steady -State Performance of Voltage Source Inverter/Synchronous Machine Drive Systems," *IEEE Tran. on Industry Application*, **20**(4), pp. 753-762, Jul./Aug. (1984)